Research Article | Vol. 12, No. 10 / 1 Oct 2022 / Optical Materials Express 4061
Optical Materials EXPRESS

Efficient and compact sol-gel TiO_2 thermo-optic microring resonator modulator

ZEQUN CHEN,[1,2,3] MAOLIANG WEI,[4,5] YE LUO,[2,3] JIALING JIAN,[2,3] YUTING YE,[2,3] YUEXIN YIN,[6] CHUNLEI SUN,[2,3] CHUYU ZHONG,[4,5] KE SI,[5] DAMING ZHANG,[6] HONGTAO LIN,[4,5] AND LAN LI[2,3,*]

[1]*Zhejiang University, Hangzhou 310027, China*
[2]*Key Laboratory of 3D Micro/Nano Fabrication and Characterization of Zhejiang Province, School of Engineering, Westlake University, Hangzhou 310024, China*
[3]*Institute of Advanced Technology, Westlake Institute for Advanced Study, Hangzhou 310024, China*
[4]*State Key Laboratory of Modern Optical Instrumentation, College of Information Science and Electronic Engineer, Zhejiang University, Hangzhou 310027, China*
[5]*MOE Frontier Science Center for Brain Science & Brain-Machine Integration, Zhejiang University, Hangzhou 310027, China*
[6]*State Key Laboratory of Integrated Optoelectronics, College of Electronic Science and Engineering, Jilin University, 2699 Qianjin Street, Changchun 130012, China*
[*]*lilan@westlake.edu.cn*

Abstract: Thermo-optic (TO) modulators play an increasingly important role in wavelength routers, lidar, optical computing, and other reconfigurable photonic systems. Highly efficient TO tunable microring resonators (MRRs) were first demonstrated based on a sol-gel TiO_2 platform in the 1310-nm waveband owing to the synergistic effect between the TiO_2 core and SU-8 cladding with both the negative thermo-optical coefficients. The MRR modulator with SU-8 polymer as the top cladding layer exhibits a thermal tuning efficiency of 33.0 pm/mW, which is more than 14 times higher than that with silica top cladding. Its rise/fall times of 9.4 us/24 us and a P_π power of 7.22 mW were achieved, indicating a relatively high TO modulator figure of merit among noncrystalline material platforms allowing monolithic integration on different substrates. These results yield a strong promise for applying the sol-gel TiO_2 platform in photonic integrated circuits and suggest a new angle of view to design compact and efficient TO modulators in wearable devices, visible/infrared communication, and biophotonic applications.

1. Introduction

The emergence of integrated photonic devices has recently received increasing attention in optical filters [1,2], visible/infrared communication [3,4], parallel optical computing [5,6], sensing [7,8], and biophotonics fields [9,10]. Thermo-optic (TO) modulators, one of the active components in integrated photonics devices, play an essential role due to their low power consumption and compact footprint [11]. The thermo-optic coefficients (TOCs) are among the most important parameters to obtain high-performance TO modulators, commonly requiring a large number. Conventional materials such as single crystal silicon (Si) (TOC: 1.86×10^{-4} K^{-1}) [1,12] and $LiNbO_3$ (TOC: 3.34×10^{-5} K^{-1}) [13] have been studied a lot and showed excellent TO performance. However, they can not be deposited and monolithically integrated on the flexible substrates for tunable photonics [14,15], strain laser [16,17], wearable sensing [18–21], and biophotonic applications [22–24]. Although silicon nitride SiN (TOC: 2.0×10^{-5} K^{-1}) [12] and amorphous silicon (3.25×10^{-4} K^{-1}) [25] can be directly patterned on the flexible substrate, there is a compromise between the film quality and deposition temperature on polymer substrates. Amorphous chalcogenide glasses [4] enable the monolithic integration of photonic

#472722 https://doi.org/10.1364/OME.472722
Journal © 2022 Received 8 Aug 2022; revised 8 Sep 2022; accepted 11 Sep 2022; published 21 Sep 2022

Optical Materials EXPRESS

devices on rigid or flexible [18,19,26] substrates at near room temperature, yet they possess a low TOC (2.5×10^{-5} K^{-1}) [11]. Polymers (TOC: ~ 10^{-4} K^{-1}) [11] with intrinsic good mechanical flexibility and low processing temperature show advantages in fabricating photonic devices [27–31]. However, the low refractive index and thermal conductivity of polymer materials lead to both the larger size and slower TO response time of the polymer modulator [26,32,33], which is undesirable in most applications, such as implantable photonic probes [22,23,34–37] requiring small wound size and fast modulation. Therefore, selecting a suitable high-index-contrast inorganic material platform is necessary for compact and efficient optical modulators.

TiO_2 has recently attracted much more attention as a promising nanophotonic material due to its low optical loss, wide operating wavelength range, high refractive index, and large negative TOC ranging between -0.5 ~ -2.4 $\times 10^{-4}$ K^{-1} [12,38,39]. Amorphous TiO_2 thin film can be prepared by different low-temperature processing techniques, such as the sol-gel method [40] and atomic layer deposition (ALD) [39], indicating its potential to be monolithically integrated on various substrates, which is an advantage for fabricating mechanically flexible integrated photonic devices [40]. Compared with the polymer waveguide, the size of the device could be much smaller when using the high-index-contrast structure consisting of a waveguide core of inorganic components, such as TiO_2 (n>2, TOC: -5.0×10^{-5} [38]), and a polymer cladding, such as SU-8 (n≈1.58, TOC: -1.87×10^{-4} [41]). Besides the device size, the high-index-contrast architecture can provide additional freedom in designing and optimizing multichannel signal modulating and routing with strong optical confinement. However, in addition to some reports about silicon-based temperature-insensitive devices using TiO_2 as the upper coating [12,42–44], TiO_2 waveguide TO modulation has rarely been reported.

In this work, we firstly demonstrated a facile strategy to construct a tunable TO MRR modulator based on a sol-gel TiO_2 platform. By introducing SU-8 as the top cladding, the TiO_2 MRR modulator exhibited remarkably enhanced TO performance (rise/fall times of 9.4 us/24 us, P_π power of 7.22 mW, thermal tuning efficiency of 33.0 pm/mW, a figure-of-merit (FOM) of 0.006 $mW^{-1}\mu s^{-1}$), owing to the synergistic effect of between TiO_2 and SU-8 with the same negative TOC. Furthermore, the desired TiO_2 MRR TO modulator also outperformed most polymer-based TO modulators as well as some silicon, SiN and $LiNbO_3$ TO modulators, which can be attributed to the higher index contrast, and higher TOC of TiO_2, respectively, thereby proving that polymeric and amorphous materials with both negative TOC may be monolithically integrated on arbitrary substrates for high-performance TO modulators.

2. Structure design and thermal simulation

The schematic cross-section and the key structural parameters of the TiO_2 modulator are shown in Fig. 1(a). The TiO_2 waveguide is a ridge waveguide with s = 100 nm, h = 150 nm, w_g = 900 nm, and a sidewall angle of 67°, which supports fundamental TE-polarized mode, as shown in Fig. 1(b). The thickness t and width w_e of the heater are selected as 100 nm and 3 μm, respectively. The separation between the heater and waveguide g is selected as 1 μm to suppress the absorption loss (Supplement 1 (Fig. (S1)). Applying a voltage on the heater, the temperature of the waveguide will change by joule heat conduction. Supplement 1, Figure (S2) shows the effective refractive index change under the different heating power. With a negative TOC in TiO_2 material, the phase tuning $\bigtriangleup\varphi$ of the waveguide is proportional to the variation in temperature $\bigtriangleup T$, which can be expressed as [45]:

$$\Delta\varphi = \frac{2\pi L}{\lambda_0}\left(\frac{dn}{dT}\right)\Delta T \tag{1}$$

where λ_0 is the free-space wavelength of the MRR, L is the length of the heater, and dn/dT is the TOC of TiO_2.

Optical Materials EXPRESS

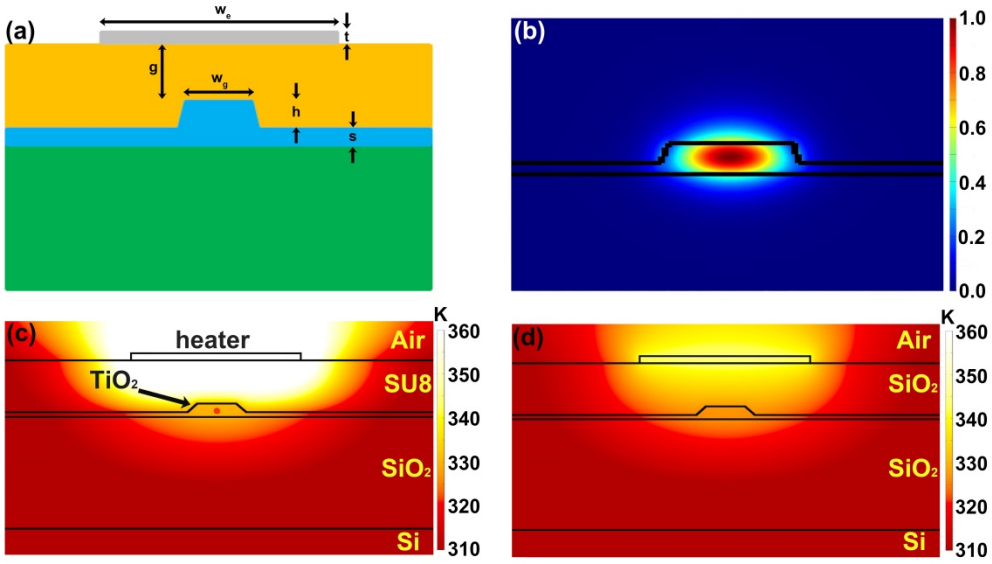

Fig. 1. (a) The schematic cross-section of the TiO_2 waveguide. (b) Fundamental TE-polarized mode of sol-gel TiO_2 waveguide at 1270 nm. Simulated temperature distribution of the TiO_2 modulator with different top/bottom cladding layers of (c) SU-8/ SiO_2 (heating power: 27.3 mW 330 K), (d) SiO_2/SiO_2 (heating power: 27.3 mW), respectively.

To study the influence of cladding materials on the temperature distribution and modulation efficiency of the TiO_2 modulator, we built a multi-physics model to analyze the TO effect for TiO_2 MRRs with different combinations of SU-8 and SiO_2 as cladding layers. The convective heat flux boundary condition was applied to conduct the thermal simulation of our devices. Figure 1(c)–1(d) show the steady-state thermal distribution in the cross-section of the devices at the same heating power of 27.3 mW. The waveguide is heated by the heater on top of the cladding. And the red mark in the center of the waveguide in Fig. 1(c) indicates the temperature sensing point. Due to the poor and superior heat conduction of the polymer and silicon substrate, respectively, the modulator suffers from local accumulated heat in the SU-8 layer and rapid heat transfer to the substrate, resulting in a slight 3K temperature increase in the center of the waveguide (330 K) with SU-8 top cladding compared with that using the silicon oxide as the top cladding.

3. Device fabrication

To verify the loss of the sol-gel TiO_2 thin film, we fabricated passive integrated optical devices consisting of grating couplers, waveguides and MRRs, as shown in Fig. 2(a). We first deposited 250 nm sol-gel TiO_2 films [40] on oxidized silicon (~2 μm) substrate. Then we coated ~400 nm thick negative electron-beam (e-beam) resist layer on the TiO_2 films and exposed the device pattern using an e-beam lithography system. The resist pattern was thermal reflowed at 120 °C for 10 s on the hotplate to remove the roughness of the pattern edge. Subsequently, the device pattern was transferred onto TiO_2 by inductively coupled plasma reactive ion etching (ICP-RIE). Finally, we deposited ~1 μm SU-8 or SiO_2 on the device as the top cladding. The as-prepared passive device is shown in Fig. 2(b). The MRR was designed to couple with a 200 μm long waveguide with a coupling gap of 400 nm and a ring resonator diameter of 80 μm. The waveguide cross-section shape is a trapezoid with a width of 900 nm on the top side, 1035 nm at the bottom edge, a height of 150 nm and a sidewall slope of approximately 67° (Fig. 2(d)) This

Optical Materials EXPRESS

waveguide structure can support the fundamental TE mode in the wavelength range of 1260-1360 nm (Fig. 1(b)).

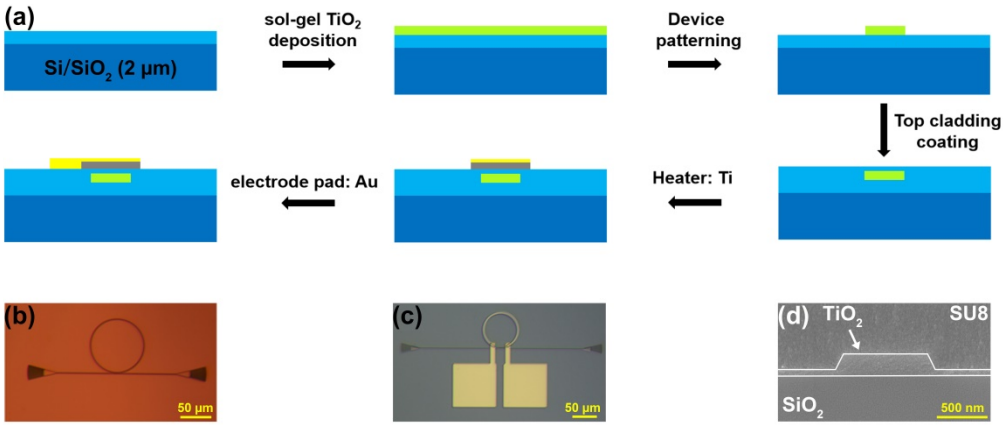

Fig. 2. TiO_2 TO MRR modulator preparation. (a) Schematic of the device fabrication process. (b) Optical microscope image of a TiO_2 MRR device. (c) Optical microscope image of a TiO_2 MRR with microheaters. (d) Cross-sectional SEM image of the TiO_2 waveguide.

To prepare the thermal-tuning MRR (Fig. 2(c)), 100 nm titanium (Ti) and 5 nm gold (Au) were first deposited above the as-prepared MRR as the metal heater by e-beam evaporation. Ti is chosen as the heating metal because of its relatively high resistivity (4.20×10^{-7} Ω•m) [46]. The 5 nm Au on 100 nm Ti is deposited to prevent Ti from oxidizing during thermal tuning. Finally, another 5 nm Ti and 100 nm Au (resistivity: 2.24×10^{-8} Ω•m) [46] were deposited as the connecting wires and probe pads.

4. Results and discussion

We characterized the optical loss of the passive sol-gel TiO_2 MRR before its thermal tunning performance was investigated. The MRRs were coupled to the input/output fibers via a pair of focusing grating couplers with 8° tilt for efficient coupling (Fig. 2(b)), in which the optical transmission spectra were collected by a broadband tunable laser system (Santec full-band TSL-550). Figure 3(a) presents a typical transmission spectrum of the TiO_2 MRR with a ring diameter of 80 μm and a coupling gap of 400 nm, showing the measured free spectral range (FSR) of 3.24 nm. The effective index of TE-polarized mode is simulated to be $n_{eff} = 1.78$ at 1273 nm, as indicated in the inset of Fig. 3(a). And Fig. 3(b) shows that the full width at half-maximum (FWHM) of sol-gel TiO_2 MRR peak at 1272.98 nm is 0.034 nm by Lorentz fit, giving the loaded Q factor of 3.74×10^4. The MRR is over coupled. The intrinsic Q factor and the propagation loss can be obtained by [42,47]:

$$Q_{int} = \frac{2Q}{1 - \sqrt{T}} \tag{2}$$

$$\alpha = \frac{\lambda_0}{Q_{int} \cdot R \cdot FSR} \tag{3}$$

where λ_0 is the wavelength of the resonance peak, T is the fraction of transmitted optical power at λ_0, R is the radius of the ring and FSR is the free spectral range, respectively. Therefore, using the MRR with a radius of 40 μm, FSR of 3.24 nm and T of 0.1 at $\lambda_0 = 1272.98$ nm, the intrinsic Q factor is 1.09×10^5 and the propagation loss is 3.9 dB/cm, comparable to the results published earlier. In our previous report, the slab sol-gel TiO_2 showed a propagation loss of 3-4 dB/cm due

Optical Materials EXPRESS

to the absorption of the remaining hydroxyl and amino groups [40]. Therefore, the additional optical loss of 0-1 dB/cm could be attributed to the roughness of the waveguide sidewall, which can be mitigated by further optimization by lithography and the etching process.

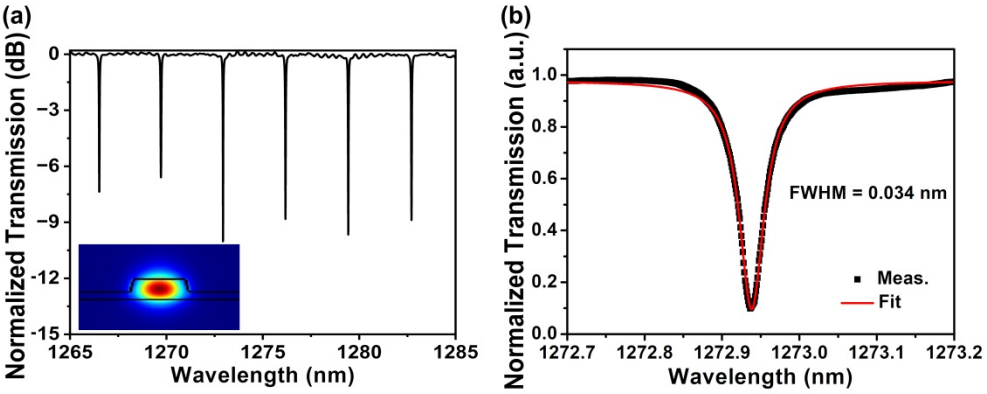

Fig. 3. (a) Normalized transmission spectrum of sol-gel TiO_2 TO MRR with an 80-μm diameter and 400-nm gap. The insert in Fig. 3(a) is the TE-polarized guided mode field at 1273 nm. (b) Close-up normalized transmission spectrum of the resonance dip at 1272.98 nm.

We designed and prepared the TiO_2 MRR TO modulators with metal heaters on top of the waveguide to verify its thermal tuning performance. The devices with the SU-8 and SiO_2 as the top cladding have been studied. For static thermal tuning measurement, a source meter was used to apply the voltage to heat the waveguide. As shown in Fig 4(a), the transmission spectrum of the TiO_2 MRR with SU-8 as the top cladding exhibits a blueshift with increasing heating power. The thermal tuning range attains 0.9 nm under a heating power of 27.3 mW (voltage of 3.0 V). Meanwhile, the thermal tuning efficiency of 33.0 ± 0.90 pm/mW was calculated by linearly fitting peak shifts with heating power (Fig. 4(b)). The FWHMs of the TiO_2 MRR dips remain unchanged, illustrating that the TiO_2 MRR has a stable optical performance, which has rarely been influenced by thermal tuning. However, the device with SiO_2 as the top cladding suffered from a higher power consumption (27.6 mW) for a small tuning range of ~ 65 pm (Fig. 4(c)), while the FWHMs of the resonance dips showed similarily negligible change (Fig. 4(d)). One reason for the higher power consumption is that the thermal conductivity of silicon oxide is an order of magnitude higher than that of SU-8; thus, more heat is localized in SU-8. Another reason is that the TOC of silicon oxide is positive while that of SU-8 and TiO_2 is negative, where a synergistic effect exists between the TiO_2 core and SU-8 cladding, resulting in reduced power consumption and increased modulation efficiency. As shown in Fig. 4(b) and Fig. 4(d), the thermal tuning efficiency of the device with SU-8 top cladding is 14 times higher than that of the device with silicon oxide top cladding (2.35 ± 0.27 pm/mW).

We further investigated the dynamic response of the sol-gel TiO_2 TO MRR modulator. A square-wave voltage of 2.0 V and 3.0 V was applied to the device with SU-8 and SiO_2 claddings, respectively. As shown in Fig. 6, the rise (10%-90%) and fall (90%-10%) times are 9.4 μs and 24 μs for the device with SU-8 cladding (Fig. 5(a)), and 14 μs and 10.7 μs for the one with SiO_2 as top cladding (Fig. 5(b)). Although the thermal conductivity of silicon oxide is higher than that of SU-8, both of them use silicon as the substrate, leading to a slight difference in thermal coupling between the two devices and the environment. Therefore, we consider that the difference in response time mainly comes from the small thermal conductivity of SU-8. Furthermore, we calculate the π-phase-shift power consumption P_π of 7.22 mW and 80.1 mW for SU8 and SiO_2

Optical Materials EXPRESS

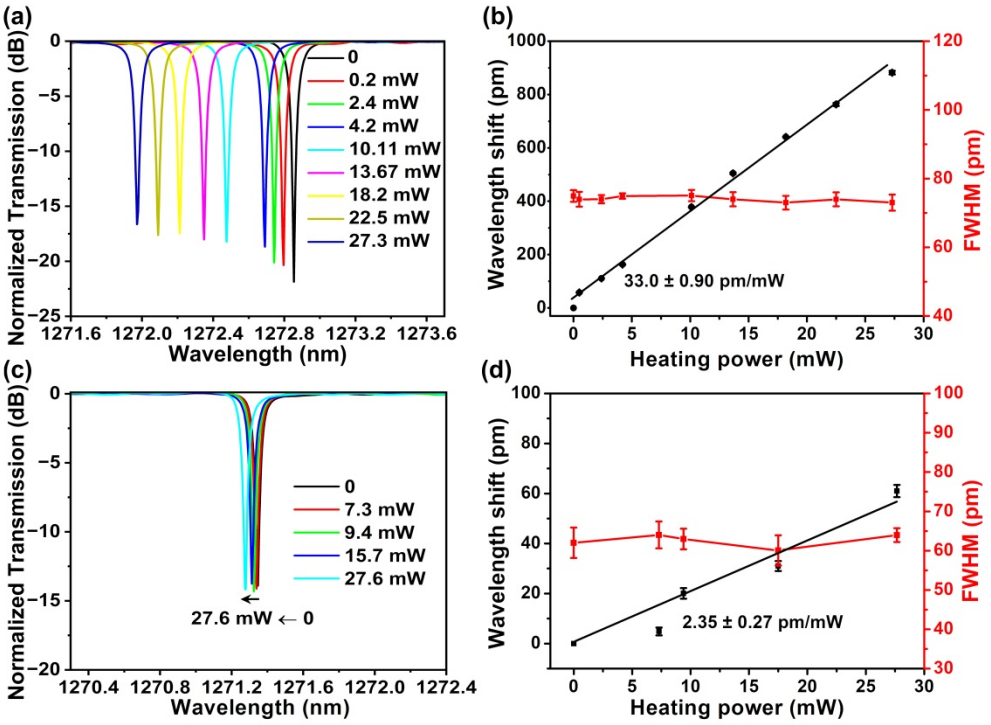

Fig. 4. Normalized optical transmission spectra of the sol-gel TiO_2 TO MRR modulator upon different heating power, with SU-8 (a) and SiO_2 (c) as the top cladding, respectively. Resonant wavelength shift and FWHM of the sol-gel TiO_2 TO MRR modulator as a function of the heating power, with SU-8 (b) and SiO_2 (d) as the top cladding, respectively. The error bar represents the standard deviation error of multiple tests.

as top cladding, respectively, according to $P_\pi = FWHM \times \pi/\eta$ [45]. In addition, a FOM of 0.006 $mW^{-1}\mu s^{-1}$ was obtained by $FOM = 1/(P_\pi \times \tau)$ [45], where τ is the response time.

We compared the performance of our proposed sol-gel TiO_2 TO MRR modulators with other reported TO modulation devices, as shown in Table 1. This indicates that our strategy has advantages in achieving TO modulators with a higher FOM than polymer MZI switches and inorganic modulators such as SiN, TiO_2 and $LiNbO_3$. TiO_2, SiN and $LiNbO_3$ possess a wide transmission window from visible to infrared regions, showing that they have similar applications in some fields. However, due to the relatively low TOC, SiN and $LiNbO_3$ TO modulators have a P_π of ~20-30 mW. Though the power consumption can be reduced by adding air trench structures, this is at the expense of dynamic response speed. Polymer materials usually have higher TOCs, but lower refractive index and slower response. Compared with TO modulators using polymeric waveguides and air trench, our device exhibits a smaller footprint and faster response speed, mainly attributed to the high index contrast and larger thermal conductive coefficient of inorganic components. And the performance can even be comparable to that of some silicon-based TO devices [48,49].

As mentioned above, sol-gel TiO_2 can be directly deposited on the flexible substrate, indicating the possibility of fabricating flexible TO modulators. Therefore, we have conducted a further simulation based on Fig. 1(c) and Fig. 1(d). As shown in Fig. 6(a), when replacing silicon oxide with SU-8 as the bottom cladding, only 6.3 mW of heating power is required to achieve 330 K (the same target temperature in Fig. 1(c)) in the TiO_2 waveguide. The main reason is

Optical Materials EXPRESS

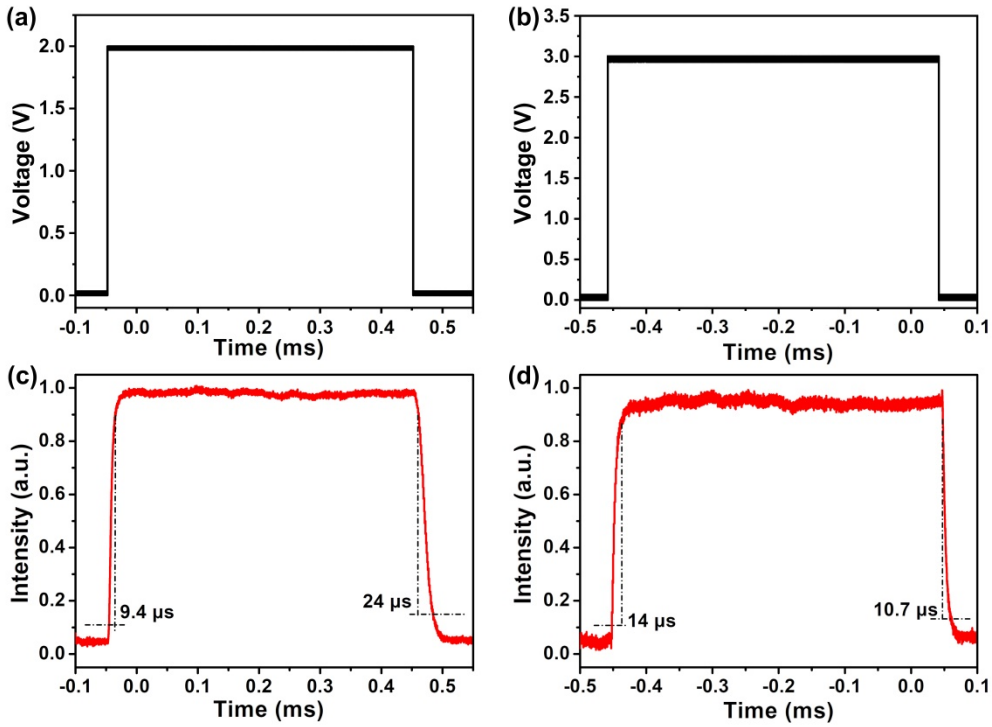

Fig. 5. The input waveform of an electrical signal applied to the sol-gel TiO_2 TO MRR modulator with (a) SU-8 and (b) SiO_2 as the cladding.Time response of sol-gel TiO_2 TO MRR modulator with (c) SU-8 and (d) SiO_2 as the cladding.

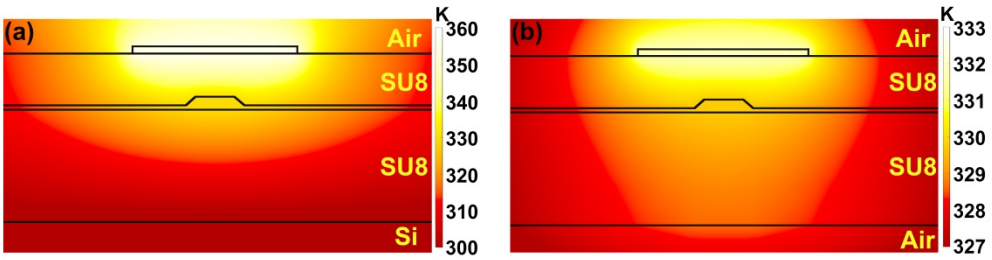

Fig. 6. Simulated temperature distribution of the TiO_2 modulator with different top/bottom cladding layers of (e) SU-8/SU-8 (heating power: 6.3 mW) on a silicon substrate and (f) SU-8/SU-8 without underlying silicon substrate (heating power: 0.55 mW), respectively.

Optical Materials EXPRESS

Table 1. Performance Comparison of Some Reported TO Modulation Devices.

Device (Device layer/Top cladding layer/Heating electrode)	Operation Wavelength (nm)	Rise/Fall time τ (μs)	Footprint (mm^2)	P_π power (mW)	FOM ($mW^{-1}\mu s^{-1}$)	Year
TiO_2 MRR / SU-8 / Ti	1272	9.4/24	0.005	7.2	0.006	this work
TiO_2 MRR / SiO_2 / Ti	1271	14.0/10.7	0.005	80.1	0.001	this work
TiO_2 MRR / air / Ti	1550	112.8/77.9	0.071	7.8	0.001	2022 [50]
$LiNbO_3$ MRR / air / NiCr	1550	60/53	0.1256	23.2	0.001	2020 [13]
SiN multi-pass waveguide / SiO_2 / TiN	561	34.5/33.5	0.82	23.0	0.001	2022 [51]
SiN multi-pass waveguide with air trench / SiO_2 / TiN	561	570/590	0.82	1.2	0.001	2022 [51]
SiN MMI / SiO_2 / Pt	488	20	-	30.0	0.002	2020 [52]
SiN MMI / SiO_2 / Pt	473	20	-	30.0	0.002	2020 [9]
SU-8 MZI / PMMA / Al	532	110/130	0.35	2.2	0.003	2020 [53]
Polymer-silica with air trench/ PMMA / Al	1550	80/80	0.33	8.9	0.001	2018 [32]
Silicon MZI / SiO_2 / TiN	2000	15/15	0.41	32.3	0.002	2019 [48]
Silicon switch / SiO_2 / TiN	2000	9.2/13.2	-	19.2	0.004	2021 [49]

attributed to the fact that the thermal conductivity coefficient of SU-8 (~ 0.2 $WK^{-1}m^{-1}$) is one order of magnitude lower than that of silica (~ 1.4 $WK^{-1}m^{-1}$) [33], preventing the heat leakage to some extent. Furthermore, after removing the silicon substrate, the device is released from the rigid substrate to become a flexible device. As a result, the same temperature in the TiO_2 waveguide (330 K) can be achieved with just 0.55 mW, suggesting a significant reduction in power consumption (Fig. 6(b)), which is advantageous for flexible TO modulators, especially in some implantable photonic devices [24,54,55]. For example, the generated heat for regular operation should be controlled as little as possible to avoid thermal damage to biological tissues. Although this may reduce the response speed to some extent, it is sufficient for multichannel biological imaging and nerve stimulation [10,24].

5. Conclusion

In summary, we have successfully demonstrated a highly efficient TO tunable MRR utilizing the sol-gel TiO_2 platform at 1310-nm-waveband. The achieved sol-gel TiO_2 TO MRR with SU-8 cladding exhibited a higher FOM than the one with silica top cladding, showing the potential for highly efficient TO modulation attributed to the synergistic effect between the TiO_2 and SU-8, which have the same negative TOCs. Moreover, both thermal simulation and the experimental result showed less power consumption when using SU-8 as the bottom cladding due to its poor heat conduction. Besides, the sol-gel TiO_2 enables monolithic integration on arbitrary substrates, including the flexible substrate at a low temperature and a smaller device size due to its high material index. Therefore, this work not only demonstrated an efficient and compact TiO_2 TO MRR, but also provided a new route for the modulation design of compact, flexible and scalable optical devices, which could be constructed by two materials systems with both large and negative or positive TOCs.

Funding. National Key Research and Development Program of China (2019YFB2203003); National Natural Science Foundation of China (12104375, 62175202); Leading Innovative and Entrepreneur Team Introduction Program of Zhejiang (2020R01005); Natural Science Foundation of Zhejiang Province (LD22F040002); MOE Frontier Science Center for Brain Science & Brain-Machine Integration, Zhejiang University.

Optical Materials EXPRESS

Acknowledgments. The authors would like to acknowledge Westlake Center for Micro/Nano Fabrication and Instrumentation, Service Center for Physical Sciences (Lin Liu and Zhen Yang's assistance in SEM characterization) at Westlake University, and ZJU Micro-Nano Fabrication Center at Zhejiang University for the facility support. The authors would also like to thank Zihao Wang, Qing Zhao and Liming Shan for their help in film preparation and characterization.

Disclosures. The authors declare no conflicts of interest.

Data availability. Data underlying the results presented in this paper are not publicly available at this time but may be obtained from the authors upon reasonable request.

Supplemental document. See Supplement 1 for supporting content.

References

1. C. Sun, Y. Yin, Z. Chen, Y. Ye, Y. Luo, H. Ma, L. Wang, M. Wei, J. Jian, R. Tang, H. Dai, J. Wu, J. Li, D. Zhang, H. Lin, and L. Li, "Tunable narrow-band single-channel add-drop integrated optical filter with ultrawide FSR," PhotoniX **3**(1), 12 (2022).
2. C. Sun, C. Zhong, M. Wei, H. Ma, Y. Luo, Z. Chen, R. Tang, J. Jian, H. Lin, and L. Li, "Free-spectral-range-free filters with ultrawide tunability across the S + C+L band," Photonics Res. **9**(6), 1013–1018 (2021).
3. G. Liang, H. Huang, A. Mohanty, M. C. Shin, X. Ji, M. J. Carter, S. Shrestha, M. Lipson, and N. Yu, "Robust, efficient, micrometre-scale phase modulators at visible wavelengths," Nat. Photonics **15**(12), 908–913 (2021).
4. H. Lin, Y. Song, Y. Huang, D. Kita, S. Deckoff-Jones, K. Wang, L. Li, J. Li, H. Zheng, Z. Luo, H. Wang, S. Novak, A. Yadav, C.-C. Huang, R.-J. Shiue, D. Englund, T. Gu, D. Hewak, K. Richardson, J. Kong, and J. Hu, "Chalcogenide glass-on-graphene photonics," Nat. Photonics **11**(12), 798–805 (2017).
5. J. Feldmann, N. Youngblood, M. Karpov, H. Gehring, X. Li, M. Stappers, M. Le Gallo, X. Fu, A. Lukashchuk, A. S. Raja, J. Liu, C. D. Wright, A. Sebastian, T. J. Kippenberg, W. H. P. Pernice, and H. Bhaskaran, "Parallel convolutional processing using an integrated photonic tensor core," Nature **589**(7840), 52–58 (2021).
6. J. Feldmann, N. Youngblood, C. D. Wright, H. Bhaskaran, and W. H. P. Pernice, "All-optical spiking neurosynaptic networks with self-learning capabilities," Nature **569**(7755), 208–214 (2019).
7. W. J. Westerveld, M. Mahmud-Ul-Hasan, R. Shnaiderman, V. Ntziachristos, X. Rottenberg, S. Severi, and V. Rochus, "Sensitive, small, broadband and scalable optomechanical ultrasound sensor in silicon photonics," Nat. Photonics **15**(5), 341–345 (2021).
8. R. Shnaiderman, G. Wissmeyer, O. Ulgen, Q. Mustafa, A. Chmyrov, and V. Ntziachristos, "A submicrometre silicon-on-insulator resonator for ultrasound detection," Nature **585**(7825), 372–378 (2020).
9. A. Mohanty, Q. Li, M. A. Tadayon, S. P. Roberts, G. R. Bhatt, E. Shim, X. Ji, J. Cardenas, S. A. Miller, A. Kepecs, and M. Lipson, "Reconfigurable nanophotonic silicon probes for sub-millisecond deep-brain optical stimulation," Nat. Biomed. Eng. **4**(2), 223–231 (2020).
10. W. D. Sacher, F. D. Chen, H. Moradi-Chameh, X. Liu, I. Felts Almog, T. Lordello, M. Chang, A. Naderian, T. M. Fowler, E. Segev, T. Xue, S. Mahallati, T. A. Valiante, L. C. Moreaux, J. K. S. Poon, and M. L. Roukes, "Optical phased array neural probes for beam-steering in brain tissue," Opt. Lett. **47**(5), 1073–1076 (2022).
11. J. Li, Y. Huang, Y. Song, L. Li, H. Zheng, H. Wang, T. Gu, K. Richardson, J. Kong, J. Hu, and H. Lin, "High-performance graphene-integrated thermo-optic switch: design and experimental validation [Invited]," Opt. Mater. Express **10**(2), 387–396 (2020).
12. B. Guha, J. Cardenas, and M. Lipson, "Athermal silicon microring resonators with titanium oxide cladding," Opt. Express **21**(22), 26557–26563 (2013).
13. X. Liu, P. Ying, X. Zhong, J. Xu, Y. Han, S. Yu, and X. Cai, "Highly efficient thermo-optic tunable micro-ring resonator based on an LNOI platform," Opt. Lett. **45**(22), 6318–6321 (2020).
14. S. M. Kamali, A. Arbabi, E. Arbabi, Y. Horie, and A. Faraon, "Decoupling optical function and geometrical form using conformal flexible dielectric metasurfaces," Nat. Commun. **7**, 11618 (2016).
15. S. C. Malek, H. S. Ee, and R. Agarwal, "Strain multiplexed metasurface holograms on a stretchable substrate," Nano Lett. **17**(6), 3641–3645 (2017).
16. M. Karl, J. M. E. Glackin, M. Schubert, N. M. Kronenberg, G. A. Turnbull, I. D. W. Samuel, and M. C. Gather, "Flexible and ultra-lightweight polymer membrane lasers," Nat Commun **9**(1), 1525 (2018).
17. H. Kung-Shu, C. Tzu-Ting, L. Po-Tsung, and S. Min-Hsiung, "Wavelength tuning by bending a flexible photonic crystal laser," J. Lightwave Technol. **31**(12), 1960–1964 (2013).
18. L. Li, H. Lin, S. Qiao, Y. Zou, S. Danto, K. Richardson, J. D. Musgraves, N. Lu, and J. Hu, "Integrated flexible chalcogenide glass photonic devices," Nat. Photonics **8**(8), 643–649 (2014).
19. L. Li, H. Lin, S. Qiao, Y.-Z. Huang, J.-Y. Li, J. Michon, T. Gu, C. Alosno-Ramos, L. Vivien, A. Yadav, K. Richardson, N. Lu, and J. Hu, "Monolithically integrated stretchable photonics," Light: Sci. Appl. **7**(2), 17138 (2018).
20. J. Michon, S. Geiger, L. Li, C. Goncalves, H. Lin, K. Richardson, X. Jia, and J. Hu, "3D integrated photonics platform with deterministic geometry control," Photonics Res. **8**(2), 194–201 (2020).
21. Y. Luo, C. Sun, H. Ma, M. Wei, J. Li, J. Jian, C. Zhong, Z. Chen, R. Tang, K. A. Richardson, H. Lin, and L. Li, "Flexible passive integrated photonic devices with superior optical and mechanical performance," Opt. Express **30**(15), 26534–26543 (2022).
22. M. Choi, J. W. Choi, S. Kim, S. Nizamoglu, S. K. Hahn, and S. H. Yun, "Light-guiding hydrogels for cell-based sensing and optogenetic synthesis in vivo," Nat. Photonics **7**(12), 987–994 (2013).

Optical Materials EXPRESS

23. Z. Chen and L. Li, "Flexible photonic probes for new-generation brain–computer interfaces," Acc. Mater. Res. **2**(5), 315–318 (2021).
24. L. C. Moreaux, D. Yatsenko, W. D. Sacher, J. Choi, C. Lee, N. J. Kubat, R. J. Cotton, E. S. Boyden, M. Z. Lin, L. Tian, A. S. Tolias, J. K. S. Poon, K. L. Shepard, and M. L. Roukes, "Integrated neurophotonics: toward dense volumetric interrogation of brain circuit activity—at depth and in real time," Neuron **108**(1), 66–92 (2020).
25. M. J. Uddin and R. Magnusson, "Guided-mode resonant thermo-optic tunable filters," IEEE Photonics Technol. Lett. **25**(15), 1412–1415 (2013).
26. L. Li, H. Lin, Y. Huang, R.-J. Shiue, A. Yadav, J. Li, J. Michon, D. Englund, K. Richardson, T. Gu, and J. Hu, "High-performance flexible waveguide-integrated photodetectors," Optica **5**(1), 44–51 (2018).
27. J. Hu, L. Li, H. Lin, P. Zhang, W. Zhou, and Z. Ma, "Flexible integrated photonics: where materials, mechanics and optics meet [Invited]," Opt. Mater. Express **3**(9), 1313–1331 (2013).
28. J. W. Reddy, M. Lassiter, and M. Chamanzar, "Parylene photonics: a flexible, broadband optical waveguide platform with integrated micromirrors for biointerfaces," Microsyst. Nanoeng. **6**(1), 85 (2020).
29. S. Huang, M. Li, S. M. Garner, M.-J. Li, and K. P. Chen, "Flexible photonic components in glass substrates," Opt. Express **23**(17), 22532–22543 (2015).
30. H. Jinno, T. Yokota, M. Koizumi, W. Yukita, M. Saito, I. Osaka, K. Fukuda, and T. Someya, "Self-powered ultraflexible photonic skin for continuous bio-signal detection via air-operation-stable polymer light-emitting diodes," Nat. Commun. **12**(1), 2234 (2021).
31. S. T. Parker, P. Domachuk, J. Amsden, J. Bressner, J. A. Lewis, D. L. Kaplan, and F. G. Omenetto, "Biocompatible Silk Printed Optical Waveguides," Adv. Mater. **21**(23), 2411–2415 (2009).
32. Q. Xu, M. Jiang, D. Niu, X. Wang, L. Wang, K. S. Chiang, and D. Zhang, "Fast and low-power thermo-optic switch based on organic-inorganic hybrid strip-loaded waveguides," Opt. Lett. **43**(20), 5102–5105 (2018).
33. M.-h. Jiang, X.-b. Wang, T.-h. Lian, D.-h. Niu, L.-l. Wang, X.-q. Sun, Z.-y. Li, and D.-m. Zhang, "Low power consumption thermo-optic switch formed by an integrated processing method," Appl. Opt. **58**(27), 7375–7378 (2019).
34. S. Nizamoglu, M. C. Gather, M. Humar, M. Choi, S. Kim, K. S. Kim, S. K. Hahn, G. Scarcelli, M. Randolph, R. W. Redmond, and S. H. Yun, "Bioabsorbable polymer optical waveguides for deep-tissue photomedicine," Nat. Commun. **7**(1), 10374 (2016).
35. W. Bai, J. Shin, R. Fu, I. Kandela, D. Lu, X. Ni, Y. Park, Z. Liu, T. Hang, D. Wu, Y. Liu, C. R. Haney, I. Stepien, Q. Yang, J. Zhao, K. R. Nandoliya, H. Zhang, X. Sheng, L. Yin, K. MacRenaris, A. Brikha, F. Aird, M. Pezhouh, J. Hornick, W. Zhou, and J. A. Rogers, "Bioresorbable photonic devices for the spectroscopic characterization of physiological status and neural activity," Nat. Biomed. Eng. **3**(8), 644–654 (2019).
36. J. Guo, C. Yang, Q. Dai, and L. Kong, "Soft and stretchable polymeric optical waveguide-based sensors for wearable and biomedical applications," Sensors **19**(17), 3771 (2019).
37. R. Fu, W. Luo, R. Nazempour, D. Tan, H. Ding, K. Zhang, L. Yin, J. Guan, and X. Sheng, "Implantable and Biodegradable Poly(l-lactic acid) Fibers for Optical Neural Interfaces," Adv. Opt. Mater. **6**(3), 1700941 (2018).
38. O. Reshef, K. Shtyrkova, M. G. Moebius, S. Griesse-Nascimento, S. Spector, C. C. Evans, E. Ippen, and E. Mazur, "Polycrystalline anatase titanium dioxide microring resonators with negative thermo-optic coefficient," J. Opt. Soc. Am. B **32**(11), 2288–2293 (2015).
39. H. Park, J. Jung, Y. Zhang, M. Liu, J. Lee, H. Noh, M. Choi, S. Lee, and H. Park, "Effects of thermally induced phase transition on the negative thermo-optic properties of atomic-layer-deposited TiO_2 films," ACS Appl. Electron. Mater. **4**(2), 651–662 (2022).
40. L. Li, P. Zhang, W.-M. Wang, H. Lin, A. B. Zerdoum, S. J. Geiger, Y. Liu, N. Xiao, Y. Zou, O. Ogbuu, Q. Du, X. Jia, J. Li, and J. Hu, "Foldable and Cytocompatible Sol-gel TiO2 Photonics," Sci. Rep. **5**(1), 13832 (2015).
41. X. Lin, T. Ling, H. Subbaraman, L. J. Guo, and R. T. Chen, "Printable thermo-optic polymer switches utilizing imprinting and ink-jet printing," Opt. Express **21**(2), 2110–2117 (2013).
42. F. Qiu, A. M. Spring, and S. Yokoyama, "Athermal and high-Q hybrid TiO_2–Si_3N_4 ring resonator via an etching-free fabrication technique," ACS Photonics **2**(3), 405–409 (2015).
43. F. Qiu, A. M. Spring, F. Yu, and S. Yokoyama, "Complementary metal–oxide–semiconductor compatible athermal silicon nitride/titanium dioxide hybrid micro-ring resonators," Appl. Phys. Lett. **102**(5), 051106 (2013).
44. S. S. Djordjevic, K. Shang, B. Guan, S. T. S. Cheung, L. Liao, J. Basak, H.-F. Liu, and S. J. B. Yoo, "CMOS-compatible, athermal silicon ring modulators clad with titanium dioxide," Opt. Express **21**(12), 13958–13968 (2013).
45. C. Zhong, H. Ma, C. Sun, M. Wei, Y. Ye, B. Tang, P. Zhang, R. Liu, J. Li, L. Li, and H. Lin, "Fast thermo-optical modulators with doped-silicon heaters operating at 2 µm," Opt. Express **29**(15), 23508–23516 (2021).
46. B. S. Mitchell, "Electrical, Magnetic, and Optical Properties of Materials," in *An Introduction to Materials Engineering and Science for Chemical and Materials Engineers* (Wiley, 2003), pp. 537–680.
47. M. Fu, Y. Zheng, G. Li, W. Yi, J. Qi, S. Yin, X. Li, and X. Guan, "Ultra-compact titanium dioxide micro-ring resonators with sub-10-µm radius for on-chip photonics," Photonics Res. **9**(7), 1416–1422 (2021).
48. L. Shen, M. Huang, S. Zheng, L. Yang, X. Peng, X. Cao, S. Li, and J. Wang, "High-performance silicon 2 × 2 high-performance silicon 2 × 2 thermo-optic switch for the 2-µm wavelength band," IEEE Photonics J. **11**(4), 1–6 (2019).
49. W. Shen, J. Du, K. Xu, and Z. He, "On-chip selective dual-mode switch for 2-µm wavelength high-speed optical interconnection," IEEE Photonics Technol. Lett. **33**(10), 483–486 (2021).

Optical Materials EXPRESS

50. H. Yu and F. Qiu, "Compact thermo-optic modulator based on a titanium dioxide micro-ring resonator," Opt. Lett. **47**(8), 2093–2096 (2022).
51. Z. Yong, H. Chen, X. Luo, A. Govdeli, H. Chua, S. S. Azadeh, A. Stalmashonak, G.-Q. Lo, J. K. S. Poon, and W. D. Sacher, "Power-efficient silicon nitride thermo-optic phase shifters for visible light," Opt. Express **30**(5), 7225–7237 (2022).
52. M. Chul Shin, A. Mohanty, K. Watson, G. R. Bhatt, C. T. Phare, S. A. Miller, M. Zadka, B. S. Lee, X. Ji, I. Datta, and M. Lipson, "Chip-scale blue light phased array," Opt. Lett. **45**(7), 1934–1937 (2020).
53. B. Lin, X. Wang, J. Lv, Y. Cao, Y. Yang, Y. Zhang, A. Zhang, Y. Yi, F. Wang, and D. Zhang, "Low-power-consumption polymer Mach–Zehnder interferometer thermo-optic switch at 532 nm based on a triangular waveguide," Opt. Lett. **45**(16), 4448–4451 (2020).
54. F. Wu, E. Stark, P.-C. Ku, K. D. Wise, G. Buzsáki, and E. Yoon, "Monolithically integrated uLEDs on silicon neural probes for high-resolution optogenetic studies in behaving animals," Neuron **88**(6), 1136–1148 (2015).
55. T.-i. Kim, G. McCall Jordan, H. Jung Yei, X. Huang, R. Siuda Edward, Y. Li, J. Song, M. Song Young, A. Pao Hsuan, R.-H. Kim, C. Lu, D. Lee Sung, I.-S. Song, G. Shin, R. Al-Hasani, S. Kim, P. Tan Meng, Y. , G. Huang, A. Omenetto Fiorenzo, R. Rogers John, and Bruchas Michael, "Injectable, cellular-scale optoelectronics with applications for wireless optogenetics," Science **340**, 211–216 (2013).